Research Square

Preprints are preliminary reports that have not undergone peer review.
They should not be considered conclusive, used to inform clinical practice,
or referenced by the media as validated information.

Research on Lateral Stability Control Strategy for Distributed Drive Electric Vehicles

Qingyi Men
Luoyang Institute of Science and Technology
Yongwei Wang
Michael_Bale_Wang@163.com
Luoyang Institute of Science and Technology
Lidong Yang
Yuxin Automotive Thermal Management Technology Co., Ltd. Xinxiang
Wensheng Ma
Henan University of Science and Technology
Guangwei Cheng
Luoyang Institute of Science and Technology

Research Article

Keywords: Distributed drive electric vehicles, Lateral stability, Sliding mode control optimization, Four-Wheel torque distribution

Posted Date: November 12th, 2026

DOI: https://doi.org/10.21203/rs.3.rs-11534989/v1

License: This work is licensed under a Creative Commons Attribution 4.0 International License.
Read Full License

Additional Declarations: No competing interests reported.

Research on Lateral Stability Control Strategy for Distributed Drive Electric Vehicles

Qingyi Men[1];Yongwei Wang[1];Lidong Yang[2];Wensheng Ma[3];Guangwei Cheng[1]

1. Luoyang Institute of Science and Technology, Luoyang, China

2. Yuxin Automotive Thermal Management Technology Co., Ltd. Xinxiang, China

3. Henan University of Science and Technology, Luoyangsss, China

Funding Statement：This work was supported by the Key scientific and technological projects in Henan Province, China (252102240100) and (262102110375)；Key Research Project Plan for Higher Education Institutions in Henan Province, China (24B4600014)

Abstract: This study aims to improve the lateral stability of Distributed Drive Electric Vehicles (DDEV) under complex driving conditions by adopting a hierarchical lateral stability control architecture. The upper level is the torque decision layer. A sliding mode controller with an additional yaw moment, optimized using the particle swarm optimization algorithm, is designed with the vehicle dynamics model as the reference framework.Ideal reference values for the yaw angular velocity and the center-of-mass side slip angle are determined based on the maximum road adhesion limit.The lower-level torque distribution layer employs a controller designed with the objective of minimizing the tire load factor, taking into account both the motor output limit and road adhesion constraints. Based on this framework, a quadratic programming-based four-wheel torque optimal distribution strategy is developed to achieve precise allocation of the additional yaw torque. The proposed control algorithm is validated through simulations on the combined CarSim and MATLAB/Simulink platform, under various road adhesion conditions and across two typical driving scenarios: dual lane-changing and serpentine driving. The results demonstrate that, when compared to the standalone SMC and the no-control baseline, the designed direct yaw moment controller and torque distribution algorithm exhibit high stability and outperform the SMC across all adhesion conditions. Furthermore, experimental validation of the lateral stability control algorithm is conducted on a HIL test platform. By comparing the tracking performance of the actual controlled values of yaw rate and center-of-mass sideslip angle against their ideal reference values, the control accuracy, real-time performance, and robustness of the controller are verified.

Keywords: Distributed drive electric vehicles, Lateral stability, Sliding mode control optimization, Four-Wheel torque distribution

1. Introduction

Distributed drive electric vehicles (DDEV), which represent a key development direction in the new energy vehicle industry, have attracted extensive attention worldwide. Driven by the “dual-carbon” goals and supportive national policies, the electric vehicle industry is accelerating its transition toward electrification and intelligent development [1]. By employing wheel-side or in-wheel motors to drive and control each wheel independently, DDEV exhibit a high degree of control freedom, rapid dynamic response, and a compact chassis layout, making them an ideal platform for implementing advanced vehicle dynamics control. Compared with traditional centralized-drive vehicles, DDEV not only eliminate complex mechanical transmission systems, thereby improving energy transmission efficiency, but also achieve a high level of chassis integration and decoupling through by-wire technologies [2]. This architecture enables precise regulation of the driving torque at each wheel, thus providing superior handling stability and safety under extreme driving maneuvers. Lateral stability is a core indicator of driving safety. Under critical conditions such as high-speed obstacle avoidance and cornering on low-adhesion roads, vehicles are highly susceptible to instability phenomena such as sideslip and spin-out [3]. Therefore, developing efficient and robust lateral stability control strategies is of both theoretical significance and engineering value for fully exploiting the dynamic potential of DDEV and ensuring occupant safety [4].

In the field of lateral stability control, various classical and advanced control methods have been proposed, mainly including proportional-integral-derivative (PID) control [5], linear quadratic regulator (LQR) [6], sliding mode control (SMC) [7], and model predictive control (MPC) [8]. Yan et al. [9] proposed a hierarchical direct yaw-moment control strategy in which the PID parameters were tuned by particle swarm optimization (PSO). By combining upper-level PID decision-making with lower-level torque allocation based on load estimation, the strategy effectively improved handling stability on low-adhesion roads. Ren et al. [10] developed an improved LQR-based yaw stability control method that considers road adhesion limits; by switching the reference model according to the linear and nonlinear tire operating regions, the method was validated through simulations with a seven-degree-of-freedom vehicle model, demonstrating effective regulation of the yaw rate and sideslip angle. Tota et al. [11] proposed an integral sliding mode controller and, through comparative validation against a conventional LQR, showed that it could effectively improve yaw damping performance and yaw rate tracking accuracy. Zhang et al. [12] designed a hierarchical direct yaw-moment control strategy, in which the upper layer combined feedforward compensation with an improved sliding mode controller to achieve accurate yaw rate

tracking, while the lower layer optimized the tire utilization ratio using quadratic programming (QP). Real-vehicle tests confirmed that this method significantly reduced tracking deviations and improved handling stability. Zhai et al. [13] proposed an integrated control strategy based on adaptive preview and MPC. Through multi-objective optimization, the front-wheel steering angle and additional yaw moment were solved cooperatively, and optimal four-wheel torque distribution was realized in combination with SMC, significantly improving path tracking accuracy and handling stability of DDEV under high-speed conditions. Chen et al. [14] developed a hybrid MPC-based yaw stability control method for DDEV. By simplifying the Magic Formula tire model into piecewise linear functions, the computational burden was reduced, and the method tracked reference signals while constraining input signals to keep in-wheel motors operating within a high-efficiency region.

To address the active safety control of DDEV under complex driving conditions, this paper proposes a hierarchical lateral stability control architecture. The upper-level controller uses a 2-degree-of-freedom (2-DOF) vehicle model as the reference, and determines the ideal reference values of yaw rate and sideslip angle by incorporating road adhesion limits. An additional yaw moment controller based on SMC is designed, and its control parameters are optimized by PSO. Furthermore, the phase plane method is introduced to quantitatively identify the vehicle stability state, allowing the final target yaw moment to be adaptively adjusted through weighting coefficients. The lower-level controller takes the minimization of the tire utilization ratio as the optimization objective; considering motor output limits and road adhesion constraints, an optimal four-wheel torque distribution strategy based on QP is designed to achieve accurate allocation of the additional yaw moment.

2. Vehicle Dynamics Model

2.1 7-DOF Vehicle Dynamics Model

A distributed drive electric vehicle is a typical multi-degree-of-freedom (multi-DOF) nonlinear complex system. Establishing a reasonable and accurate simplified model is essential for studying the lateral stability of DDEV. To balance algorithm real-time performance and estimation accuracy, and to account for the coupling characteristics of tire longitudinal and lateral forces, this paper establishes a 7-DOF vehicle dynamics model. The model includes three rigid-body planar motion degrees of freedom (longitudinal, lateral, and yaw) and the rotational motion of the four wheels. It can reflect the influence of wheel slip characteristics on vehicle attitude more realistically while fully characterizing the nonlinear dynamic features of the vehicle [15]. Based on this model, the following assumptions are made:

(1) The origin of the vehicle coordinate system coincides with the vehicle center of gravity (CG).

(2) The vehicle is modeled as a rigid body with four independently controllable wheels, and the elastic deformation of the vehicle body is neglected.

(3) The mechanical and steering characteristics of the four tires are identical.

(4) The effects of vertical motion and suspension deformation on the vehicle dynamics are ignored.

(5) The effects of aerodynamic drag and grade resistance on vehicle motion are not considered.

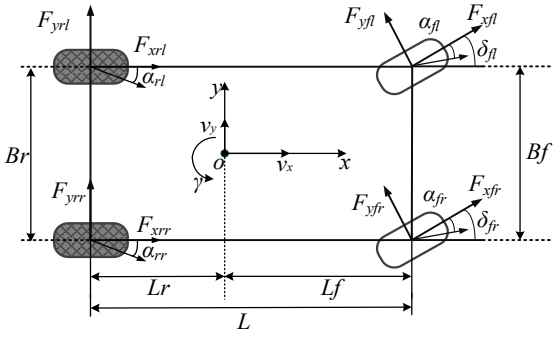


Fig. 1 7-DOF vehicle dynamics model

The 7-DOF vehicle dynamics model is illustrated in Fig. 1. Let xOy denote the vehicle coordinate system, where the x-axis and y-axis represent the longitudinal and lateral directions, respectively, with the positive directions aligned with vehicle motion. According to Newton's second law, the equations of motion are expressed as follows:

Longitudinal motion:

$$\begin{cases} ma_x = F_{xfl}\cos\delta_{fl} + F_{xfr}\cos\delta_{fr} - F_{yfl}\sin\delta_{fl} - F_{yfr}\sin\delta_{fr} + F_{xrl} + F_{xrr} \\ \dot{v}_x = a_x + v_y\gamma \end{cases} \tag{1}$$

Lateral motion:

$$\begin{cases} ma_y = F_{xfl}\sin\delta_{fl} + F_{xfr}\sin\delta_{fr} + F_{yfl}\cos\delta_{fl} + F_{yfr}\cos\delta_{fr} + F_{yrl} + F_{yrr} \\ \dot{v}_y = a_y - v_x\gamma \end{cases} \tag{2}$$

Yaw motion:

$$\begin{cases} M = \dfrac{B_f}{2}(F_{xfr}\cos\delta_{fr} - F_{yfr}\sin\delta_{fr} - F_{xfl}\cos\delta_{fl} + F_{yfl}\sin\delta_{fl}) \\ \quad + L_f(F_{xfl}\sin\delta_{fl} + F_{xfr}\sin\delta_{fr} + F_{yfl}\cos\delta_{fl} + F_{xfr}\sin\delta_{fr} + F_{yfr}\cos\delta_{fr}) \\ \quad + \dfrac{B_r}{2}(F_{xrr} - F_{xrl}) - L_r(F_{yrl} - F_{yrr}) \\ \dot{\gamma} = \dfrac{1}{I_z}M \end{cases} \tag{3}$$

where v_x and v_y are the longitudinal and lateral velocities, respectively; a_x and a_y are the longitudinal and lateral accelerations, respectively; I_z is the moment of inertia about the z-axis; γ is the yaw rate; M is the yaw moment; F_{xij} and F_{yij} are the longitudinal and lateral forces of the corresponding wheel, respectively, where in the subscript ij, the first character f/r denotes the front/rear axle, and the second character l/r denotes the left/right wheel; L_f and L_r are the distances from the center of gravity (CG) to the front and rear axles, respectively; B_f and B_r are the track widths of the front and rear axles, respectively; m is the full-vehicle mass; and δ_{fl} and δ_{fr} are the steering angles of the front-left and front-right wheels, respectively.

2.2 Tire Model

During vehicle motion, the driving, braking, and lateral forces are all transmitted through the tires, and the tires are also the direct actuators of torque distribution in lateral stability control. Therefore, the mathematical characteristics and dynamic behavior of tires have a significant influence on vehicle lateral stability control. Establishing an accurate tire model that captures the nonlinear characteristics of tire forces is a prerequisite for this study. In this paper, the Dug off nonlinear tire model is adopted. This analytical tire model requires only a few parameters and has a simple structure [16–17].

$$F_{yij} = \mu F_{zij} C_y \frac{\tan(\alpha_{ij}) f(L)}{1-\lambda_{i_j}} \tag{4}$$

$$f(L) = \begin{cases} 1, L \geq 1 \\ L(2-L), L < 1 \end{cases} \tag{5}$$

$$L = \frac{(1-\lambda_{i_j})}{2\sqrt{C_x^2\lambda_{ij}^2 + C_y^2\tan^2\alpha_{ij}}}\left(1 - \varepsilon \cdot v_{xij} \cdot \sqrt{C_x^2\lambda_{ij}^2 + C_y^2\tan^2\alpha_{ij}}\right) \tag{6}$$

where λ is the slip ratio; C_x is the longitudinal tire stiffness; C_y is the lateral tire stiffness; α is the tire slip angle; μ is the road adhesion coefficient; ε is the speed

influence factor used to describe the effect of slip speed on the tire force; and L is a nonlinear characteristic parameter used to describe tire slip.

$$\begin{aligned}\lambda_{i_j} &= \frac{\omega_{ij}R_e - v_{ij}}{v_{ij}} = \frac{\omega_{ij}R_e}{v_{ij}} - 1 < 0(\text{brake}) \\ \lambda_{i_j} &= \frac{\omega_{ij}R_e - v_{ij}}{R_e v_{ij}} = 1 - \frac{v_{ij}}{\omega_{ij}R_e} > 0(\text{drive})\end{aligned} \tag{7}$$

The calculation formula for the wheel slip angle is expressed as follows:

$$\left.\begin{aligned}\alpha_{fr,fl} &= \delta_{fr,fl} - \arctan\left(\frac{v_y + L_f\gamma}{v_x \pm \frac{B_f}{2}\gamma}\right) \\ \alpha_{rl,rr} &= -\arctan\left(\frac{v_y - L_r\gamma}{v_x \mp \frac{B_r}{2}\gamma}\right)\end{aligned}\right\} \tag{8}$$

Vertical tire force:

$$\left.\begin{aligned}F_{zfl,zfr} &= L_r\left(\frac{mg}{2L} \mp \frac{ma_y h_g}{B_f L}\right) - \frac{ma_x h_g}{2L} \\ F_{zrl,zrr} &= L_f\left(\frac{mg}{2L} \mp \frac{ma_y h_g}{B_r L}\right) + \frac{ma_x h_g}{2L}\end{aligned}\right\} \tag{9}$$

3. Controller Design

3.1 2-DOF Dynamics Model

To simplify computation and analysis, a 2-DOF vehicle dynamics model is established. Compared with complex multi-DOF models, the 2-DOF model can more intuitively and effectively capture the fundamental lateral and yaw dynamic characteristics of the vehicle while offering higher computational efficiency. The ideal sideslip angle and yaw rate calculated from this model are used as real-time references, helping the stability control system derive effective control actions. Therefore, this model is adopted as the ideal reference model, as shown in Fig. 2.

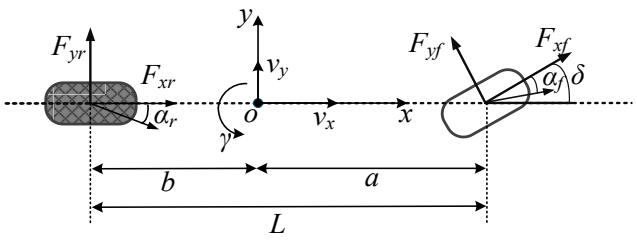


Fig. 2 2-DOF Vehicle Model

In the 2-DOF vehicle model, the equilibrium equations for the lateral force and yaw moment are expressed as follows:

$$m\left(\dot{v}_y + v_x r\right) = F_{yf}\cos\delta + F_{yr} \tag{10}$$

$$I_z\dot{r} = aF_{yf}\cos\delta - bF_{yr} \tag{11}$$

where F_{yf} is the resultant lateral force of the front wheels; and F_{yr} is the resultant lateral force of the rear wheels.

Under normal driving conditions, the front-wheel steering angle typically remains within a small range, during which the lateral forces of the front and rear wheels exhibit a linear relationship with the wheel slip angles. Considering only the steady-state cornering condition of the vehicle, the vehicle yaw rate remains constant, and the vehicle sideslip angle is also a constant value, satisfying $\dot{v}_y = 0$ and $\dot{r} = 0$. By substituting these conditions into the above equations, the expressions for the ideal vehicle sideslip angle β_d and the ideal yaw rate r_d under steady state can be derived as follows:

$$\begin{cases} \beta_d = \dfrac{b/(a+b) + mav_x^2/(a+b)^2 k_r\big)}{1+Kv_x^2}\delta \\ r_d = \dfrac{v_x\delta/(a+b)}{1+Kv_x^2} \end{cases} \tag{12}$$

where K is the stability factor of the vehicle and $K = \dfrac{m}{(a+b)^2}\left(\dfrac{a}{k_r} - \dfrac{b}{k_f}\right)$.

The derivation of the above ideal parameters is based on the assumption of linear tire characteristics. When the vehicle is driven under limit conditions, the tire forces tend to saturate and enter the nonlinear operating region, where the linear tire model is no longer applicable. Moreover, in practice, the proportion of lateral acceleration allowed by road adhesion is typically taken as 85% [18]. Therefore, considering road adhesion utilization, the constrained ideal yaw rate and sideslip angle are expressed as:

$$|\gamma_d| \le \frac{\mu g}{v_x} \tag{13}$$

$$|\beta_d| \le \mu g\left(\frac{b}{v_x^2}+\frac{ma}{k_r(a+b)}\right) \tag{14}$$

In summary, the final outputs β_d and r_d of the 2-DOF vehicle reference model in this paper are determined as the minimum values between those under the aforementioned ideal state and those under the constraints of road adhesion conditions, which are expressed as follows:

$$\beta_d = \min\left\{\left|\frac{b/(a+b)+mav_x^2/\left((a+b)^2k_r\right)}{1+Kv_x^2}\delta\right|, \left|0.85\mu g\left(\frac{b}{v_x^2}+\frac{ma}{k_r(a+b)}\right)\right|\right\}$$

$$r_d = \min\left\{\left|\frac{v_x\delta/(a+b)}{1+Kv_x^2}\right|, \left|0.85\frac{\mu g}{v_x}\right|\right\}$$

3.2 Upper-Level Controller

DDEV exhibit strong nonlinear characteristics during driving. Sliding mode control (SMC) is characterized by its discontinuous control action and possesses strong robustness against model uncertainties and external disturbances. Therefore, SMC is widely applied in the research of vehicle dynamics control.

By substituting the additional yaw moment ΔM into the aforementioned reference model, the equation is expressed as follows:

$$\begin{cases}\dot{\gamma} = \dfrac{aK_f - bK_r}{I_z}\beta + \dfrac{a^2K_f + b^2K_r}{I_z v_x}\gamma - \dfrac{aK_f}{I_z}\delta + \dfrac{\Delta M}{I_z} \\ \dot{\beta} = \dfrac{K_f + K_r}{mv_x}\beta + \left(\dfrac{aK_f - bK_r}{mv_x^2} - 1\right)\gamma - \dfrac{K_f}{mv_x}\delta\end{cases} \tag{15}$$

3.2.1 Yaw Rate Tracking SMC Design

During the yaw rate tracking control, the yaw rate tracking error and its rate of change are defined as follows:

$$e_r = r - r_d \tag{16}$$

$$\dot{e}_r = \dot{r} - \dot{r}_d \tag{17}$$

Based on the aforementioned error variables, the sliding surface is designed as:

$$s_r = e_r + c_1\dot{e}_r \tag{18}$$

where s_r is the yaw rate sliding mode variable; and c_1 is the error weighting coefficient, which is greater than 0.

In the sliding mode reaching phase, the exponential reaching law is adopted $\dot{s}_r = -\varepsilon_1 sgn(s) - k_1 s$, where $-k_1 s$ represents the exponential reaching term, and the value of k_1 determines the reaching rate of the system toward the sliding surface; $-\varepsilon_1 sgn(s)$ represents the constant rate reaching term, which ensures that the system reaches the sliding surface within a finite time.

Taking the derivative of the sliding surface yields:

$$\begin{aligned} \dot{s}_r &= \dot{e}_r + c_1\ddot{e}_r = (\dot{r} - \dot{r}_d) + c_1(\ddot{r} - \ddot{r}_d) \\ &= \dot{r}\frac{c_1(a^2k_f + b^2k_r)}{I_z V_x} + \frac{c_1(ak_f - bk_r)}{I_z}\dot{\beta} \\ &\quad - \frac{c_1 ak_f}{I_z}\dot{\delta} - \dot{r}_d - c_1\ddot{r}_d + \frac{c_1\Delta\dot{M}_r}{I_z} = X + \frac{c_1\Delta\dot{M}_r}{I_z} \end{aligned} \tag{19}$$

By substituting the exponential reaching law into the aforementioned derivative of the sliding surface, and replacing the sign function $sat(\cdot)$ with the saturation function $sgn(\cdot)$ to suppress chattering, the additional yaw moment control law is finally derived as follows:

$$\Delta M_r = -\frac{I_z}{c_1}\int\left(\varepsilon_1 \mathrm{sat}(s) + k_1 s + X\right)dt \tag{20}$$

3.2.2 Vehicle Sideslip Angle Tracking SMC Design

To meet the requirements of the vehicle sideslip angle tracking control, the tracking error and its rate of change are defined as follows:

$$e_\beta = \beta - \beta_d \tag{21}$$

$$\dot{e}_\beta = \dot{\beta} - \dot{\beta}_d \tag{22}$$

$$s_\beta = e_\beta + c_2\dot{e}_\beta \tag{23}$$

Taking the derivative of the sliding surface yields:

$$\begin{aligned} \dot{s}_\beta = \dot{e}_\beta + c_2\ddot{e}_\beta = c_2 &\left\{\frac{k_f + k_r}{mV_x}\left[\frac{k_f + k_r}{mV_x}\beta + \left(\frac{ak_f - bk_r}{mV_x^2} - 1\right)r - \frac{k_f}{mV_x}\delta\right]\right. \\ &\left. + \left(\frac{ak_f - bk_r}{mV_x^2} - 1\right)\left(\frac{ak_f - bk_r}{I_z}\beta + \frac{a^2k_f + b^2k_r}{I_z V_x}r - \frac{ak_f}{I_z}\delta\right) - \dot{\beta}_d - c_2\ddot{\beta}_d\right\} \\ &+ \left(\frac{ak_f - bk_r}{mV_x^2} - 1\right)\frac{\Delta M_\beta}{I_z} = Y + c_2\left(\frac{ak_f - bk_r}{mV_x^2} - 1\right)\frac{\Delta M_\beta}{I_z} \end{aligned} \tag{24}$$

The additional yaw moment is derived as follows:

$$\Delta M_{\beta} = -\frac{I_z}{c_2 + \left(\frac{ak_f - bk_r}{mV_x^2} - 1\right)} \int \left(\varepsilon_1 \mathrm{sat}(s) + k_1 s + Y\right) dt \tag{25}$$

The verification of Lyapunov stability is presented as follows:

$$\dot{V}_1 = s\dot{s} = s_r \dot{s}_r = s_r(-\varepsilon_1 \operatorname{sgn}(s_r) - k_1 s_r) \le 0 \tag{26}$$

Therefore, the designed control system satisfies the Lyapunov stability condition. The stability of the sideslip angle controller can be proved in the same manner, ensuring that the entire system reaches the sliding surface within a finite time.

Since the parameter settings in the above equations are not unique, a particle swarm optimization (PSO) strategy is designed to determine the optimal control parameters.

The parameter vector to be optimized is defined as $E = [c_1, c_2, \varepsilon_1, \varepsilon_2, k_1, k_2]$. The standard PSO algorithm is adopted for the optimization, and the process is as follows:

(1) Initialization: Randomly generate M particles in the search space, where the position of each particle represents a parameter vector E, and randomly initialize their velocities.

(2) Evaluation: For each particle, substitute its corresponding parameters into the controller, and run the CarSim-Simulink co-simulation under the set driving conditions.

(3) Update: Compare and update the historical best position P_{best} of each particle, as well as the global best position g_{best} of the entire swarm.

(4) Iteration: According to the velocity and position update formulas of PSO, iteratively update the entire particle swarm as follows:

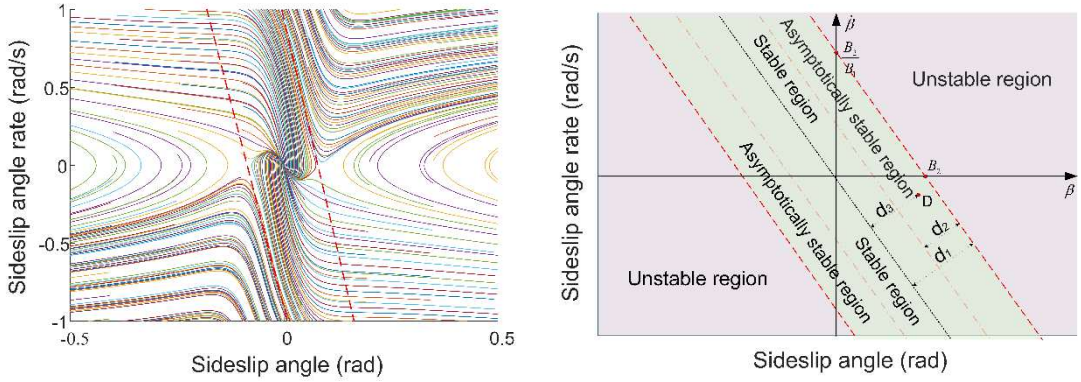
$$\begin{cases} v_i^{k+1} = \omega v_i^k + b_1 r_1 \left(p_{best,i} - E_i^k\right) + b_2 r_2 \left(g_{best} - E_i^k\right) \\ E_i^{k+1} = E_i^k + v_i^{k+1} \end{cases} \tag{27}$$

where ω is the inertia weight; b_1 and b_2 are the learning factors; r_1 and r_2 are random numbers; i denotes the i-th particle; k is the current iteration number; v_i^k is the velocity of the i-th particle at the k-th iteration; and E_i^k is the position of the i-th particle at the k-th iteration.

3.3 Research on Phase Plane Stability Strategy

As a classical graphical analysis tool for stability control, the phase plane method is widely used to study the state trajectory evolution of low-order linear and nonlinear systems because of its intuitive graphical representation. There are mainly two

commonly used phase plane portraits: the $\beta-\dot{\beta}$ and $\beta-\gamma$ phase plane portraits. When the driving speed of the vehicle changes, the stable region of its $\beta-\gamma$ phase plane is greatly affected and varies significantly. Therefore, the $\beta-\dot{\beta}$ phase plane portrait is selected in this paper to evaluate the lateral stability of the driven vehicle.



(a) $\beta-\dot{\beta}$ phase plane portrait (b) Phase plane stable region division

Fig. 3 Phase plane portrait

Based on road adhesion coefficients ranging from 0.1 to 0.8, this paper establishes a stability and boundary parameter table for the vehicle sideslip angle and its rate of change, which serves as the basis for subsequent stability evaluation, as shown in Tab.1.

Tab.1 Stability domain boundary coefficients under road adhesion coefficients of 0.1~0.8

μ	0.1	0.2	0.3	0.4	0.5	0.6	0.7	0.8
B_1	5.122	5.974	6.811	7.634	8.092	8.510	8.907	9.281
B_2	0.185	0.316	0.479	0.674	0.821	0.977	1.143	1.296

To mitigate the intervention-induced chattering caused by applying the control strategy immediately after the stability state is evaluated, and to enhance the robustness of the stability evaluation near the phase plane boundaries, an asymptotically stable region is introduced between the traditional stable region and the unstable region, as shown in Fig. 3(b). A weighting coefficient ρ is introduced to represent the width of the asymptotically stable region. Its boundary equation is given by:

$$\left|\dot{\beta}+B_1\beta\right|=\rho B_2,\ \ 0<\rho<1 \tag{28}$$

Within the asymptotically stable region, assume there exists a point D$(\beta_d,\dot{\beta}_d)$, where the total width of the stable region and the asymptotically stable region is d_1, the width of the asymptotically stable region is d_2, and the width from point D to the stable center boundary is d_3. Accordingly, the asymptotically stable region can be

quantitatively defined, and the respective expressions are given as follows:

$$d_1 = \frac{|B_2|}{\sqrt{1+B_1^2}} \tag{29}$$

$$d_2 = d_1 - \frac{|\rho B_2|}{\sqrt{1+B_1^2}} = \frac{|(1-\rho)B_2|}{\sqrt{1+B_1^2}} \tag{30}$$

To achieve coordinated control within the asymptotically stable region, the adaptive adjustment coefficient Φ for the asymptotically stable region is defined as follows:

$$\Phi = \frac{d_3 - (d_1 - d_2)}{d_2} = \frac{\left|\dot{\beta}_d + B_2\beta_d - \rho B_2\right|}{|(1-\rho)B_2|} \tag{31}$$

Therefore, based on the partitioned boundaries of the $\beta - \dot{\beta}$ phase plane method, the vehicle stability control weight coefficient ξ is determined as follows:

$$\xi = \begin{cases} 0, & \left|\dot{\beta}_d + B_1\beta_d\right| < \rho B_2 \\ \Phi, & \rho B_2 \le \left|\dot{\beta}_d + B_1\beta_d\right| \le B_2 \\ 1, & \left|\dot{\beta}_d + B_1\beta_d\right| > B_2 \end{cases} \tag{32}$$

Integrating the aforementioned weight coefficient, the final additional yaw moment required to maintain lateral stability is designed as follows:

$$\Delta M = (1-\xi)\Delta M_\beta + \xi \Delta M_\gamma \tag{33}$$

When the vehicle is located in the stable region, the control objective prioritizes the sideslip angle to enhance driving smoothness; when the vehicle operates in the asymptotically stable region, the yaw rate and sideslip angle are coordinated through the dynamic weight factor to achieve a balance between smoothness and stability; if the vehicle falls into the unstable region, priority is given to the forced intervention of yaw rate control, thus guaranteeing vehicle stability by rapidly suppressing the instability tendency.

3.4 Design of the Lower-Level Optimal Torque Allocation Controller

The lower-level torque allocation controller plays a critical role in vehicle stability control by distributing the upper-level yaw moment to each wheel under multiple constraints. Among even, dynamic, and optimal allocation strategies, optimal allocation is preferred because of its flexible objective and constraint design, high control precision, and superior real-time performance. Subject to equality and inequality constraints, the objective function minimizes the tire adhesion utilization rate to

enhance the vehicle stability margin, and the QP method is used for torque allocation.

Since the additional yaw moment in the proposed EV model is controlled by the longitudinal driving or braking forces of the four wheels, the influence of lateral wheel forces is neglected, yielding the following optimal objective function:

$$\min J = \sum_{i=1}^{4} \frac{F_{xi}^2}{(\mu_i F_{zi})^2} \tag{34}$$

Excessive tire adhesion utilization rate risks vehicle instability; thus, setting its minimization as the objective function effectively enhances vehicle stability. Subject to the constraints of longitudinal force and additional yaw moment, the influence of the front-wheel steering angle is neglected due to its small magnitude at high speeds.

$$\begin{cases} F_x = F_{xfl} + F_{xfr} + F_{xrl} + F_{xrr} \\ \Delta M = \dfrac{B}{2R_e}\left(-T_{fl} + T_{fr} - T_{rl} + T_{rr}\right) \end{cases} \tag{35}$$

Subject to the maximum motor torque and road adhesion constraints, and restricted by the physical limits of the in-wheel motors' external characteristics.

$$-T_{\max} \le T_i \le T_{\max} \tag{36}$$

$$-\mu F_{zj} \le F_{xj} \le \mu F_{zj} \tag{37}$$

The above equality and inequality constraints are transformed into a QP formulation as follows:

$$\begin{cases} \min J = \dfrac{1}{2} x^T H x + f^T x_{rr} \\ \text{s.t. } A_{eq} x = B_{eq} \quad Ax \le b \quad LB \le x \le UB \end{cases} \tag{38}$$

where f is the linear coefficient vector of the objective function; LB and UB denote the lower and upper bounds of the optimization variable x; and A_{eq}, B_{eq}, A, and b represent the coefficient matrices and vectors corresponding to the constraints.

Based on the expressions of the objective function and constraints, the positive definite Hessian matrix H, the equality constraint coefficient matrix A_{eq}, and the constant vector B_{eq} in the standard QP formulation are determined as follows:

$$H=\mathrm{diag}\left(\frac{2}{\left(\mu_{fl}F_{zfl}\right)^2},\frac{2}{\left(\mu_{fr}F_{zfr}\right)^2},\frac{2}{\left(\mu_{rl}F_{zrl}\right)^2},\frac{2}{\left(\mu_{rr}F_{zrr}\right)^2}\right) \tag{39}$$

$$A_{eq}=\begin{pmatrix}1 & 1 & 1 & 1\\ -\frac{B}{2} & \frac{B}{2} & -\frac{B}{2} & \frac{B}{2}\end{pmatrix} \tag{40}$$

$$B_{eq}=\left[T_x,\Delta M\right]^T \tag{41}$$

By applying equality constraint elimination to reduce the variable dimensionality and simplify the solution logic, the optimal driving torque for each in-wheel motor can be obtained as:

$$\begin{cases} T_{fl}=\dfrac{T_x}{2}-\dfrac{\Delta M}{B}R_w-\dfrac{\left(\dfrac{T_x}{2}-\dfrac{\Delta M}{B}R_w\right)\left(\mu_{rl}F_{zrl}\right)^2}{\left(\mu_{fl}F_{zfl}\right)^2+\left(\mu_{rl}F_{zrl}\right)^2} \\ T_{fr}=\dfrac{T_x}{2}+\dfrac{\Delta M}{B}R_w-\dfrac{\left(\dfrac{T_x}{2}+\dfrac{\Delta M}{B}R_w\right)\left(\mu_{rl}F_{zrr}\right)^2}{\left(\mu_{fl}F_{zfr}\right)^2+\left(\mu_{rl}F_{zrr}\right)^2} \\ T_{rl}=\dfrac{\left(\dfrac{T_x}{2}-\dfrac{\Delta M}{B}R_w\right)\left(\mu_{rl}F_{zrl}\right)^2}{\left(\mu_{fl}F_{zfl}\right)^2+\left(\mu_{rl}F_{zrl}\right)^2} \\ T_{rr}=\dfrac{\left(\dfrac{T_x}{2}+\dfrac{\Delta M}{B}R_w\right)\left(\mu_{rl}F_{zrr}\right)^2}{\left(\mu_{fl}F_{zfr}\right)^2+\left(\mu_{rl}F_{zrr}\right)^2} \end{cases} \tag{42}$$

4. Analysis of Offline Simulation and Hardware-in-the-Loop Results

The test vehicle in this study is a B-class vehicle, with its parameters detailed in Tab.2:

Tab.2 Vehicle parameters

Parameter	Symbol	Value
Vehicle mass (kg)	m	1412
Sprung mass (kg)	ms	1270
Distance from CG to front axle (m)	Bf	1.015
Distance from CG to rear axle (m)	Br	1.895
Front track width (m)	Lf	1.675
Rear track width (m)	Lr	1.675
CG height (m)	hg	0.54

Yaw moment of inertia (kg·m^2)	Iz	1536.7
Wheel radius (m)	Re	0.325

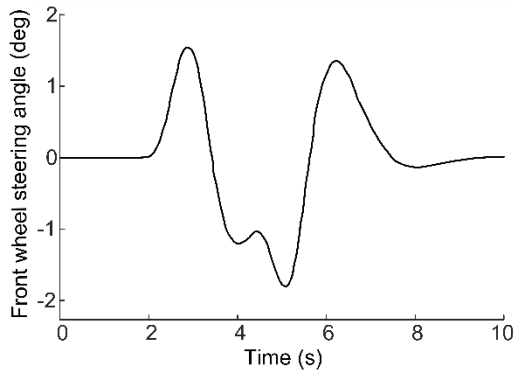
4.1 Offline Simulation

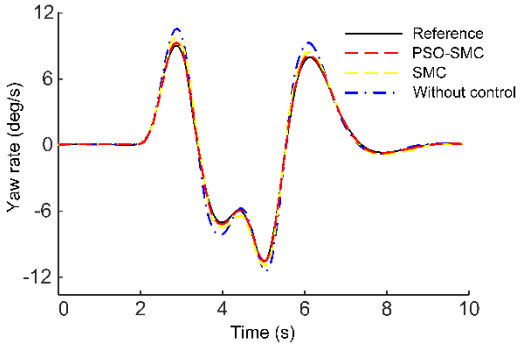
The control algorithm is verified via a CarSim and MATLAB/Simulink co-simulation platform. Double lane change (DLC) and slalom scenarios are designed under high and low road adhesion conditions, respectively. By comparing the proposed PSO-SMC, standard SMC, and the uncontrolled condition, the effectiveness and practicality of the direct yaw moment controller and the torque allocation algorithm are validated. For further quantitative analysis, the maximum estimation error E_{MAX} and root mean square error E_{RMS} are employed.

$$E_{RMS} = \sqrt{\frac{1}{N}\sum_{h=1}^{N}\left(\mathrm{x}_h - x_h\right)}$$
$$E_{MAX} = \max\left|\mathrm{x}_h - x_h\right| \tag{43}$$

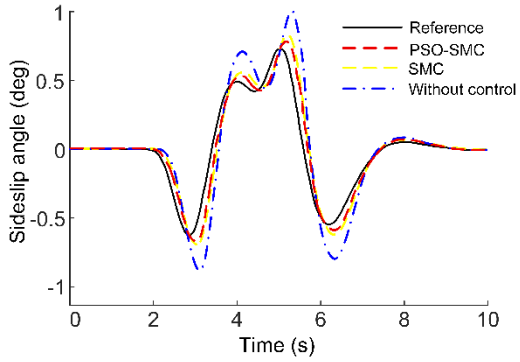
4.1.1 DLC Scenario

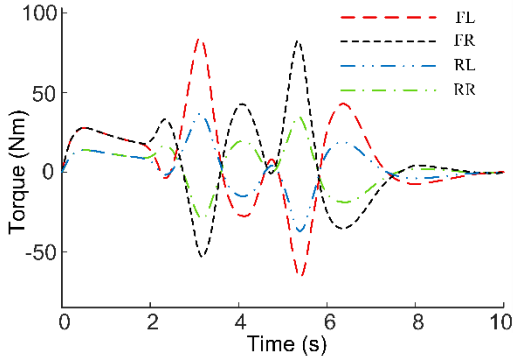
The DLC scenario simulates obstacle avoidance or overtaking maneuvers for high-speed distributed drive EVs and is suitable for validating the lateral stability control system. The initial speed is set to 85 km/h, and the road adhesion coefficients are set to 0.8 and 0.3. The simulation results are presented in Figs. 4 and 5.





(a) Wheel angle (b) Yaw rate





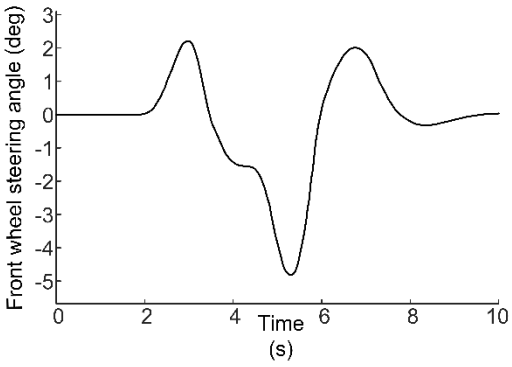
(c) CG sideslip angle (d) Optimal allocated torque

Fig. 4 Simulation under DLC scenario ($\mu = 0.8$)

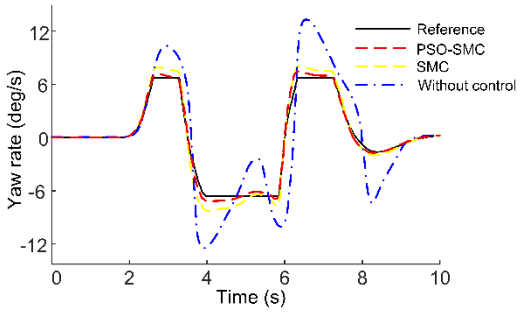
Tab.3 DLC scenario errors ($\mu = 0.8$)

Error	Control algorithm	Yaw rate (deg/s)	CG sideslip angle (deg)
E_{MAX}	SMC	0.453	0.095
	PSO-SMC	0.296	0.050
E_{RMS}	SMC	0.212	0.038
	PSO-SMC	0.183	0.025

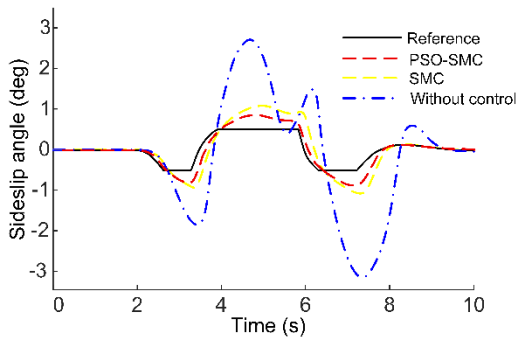
Fig. 4(a) shows the front steering angle input, which provides typical steering dynamic excitation for the vehicle lateral dynamics. The yaw rate and CG sideslip angle responses in Figs. 4(b) and 4(c) show improved tracking performance after applying control. Based on Tab. 3, compared with SMC, the proposed PSO-SMC effectively reduces E_{MAX}. Furthermore, the E_{RMS} of the yaw rate and CG sideslip angle are decreased by 13.7% and 34.2%, respectively. Fig. 4(d) illustrates the optimal allocated torque of the four wheels. The lower-level controller achieves differentiated coordinated regulation of the four-wheel torques to accurately generate the desired additional yaw moment from the upper layer, ensuring the stable execution of the control strategy.



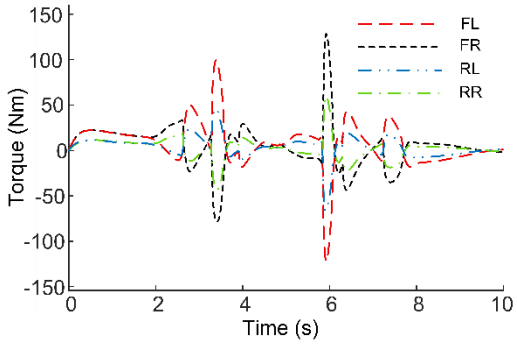
（a）Front wheel steering angle



（b）Yaw rate



(c) CG sideslip angle



(d) Optimal allocated torque

Fig. 5 Simulation under DLC scenario (μ =0.3)

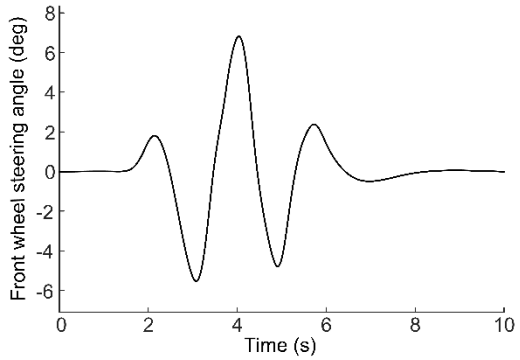
Tab.4 DLC scenario errors (μ =0.3)

Error	Control algorithm	Yaw rate (deg/s)	CG sideslip angle (deg)
E_{MAX}	SMC	0.906	0.545
	PSO-SMC	0.638	0.326
E_{RMS}	SMC	0.439	0.197
	PSO-SMC	0.297	0.124

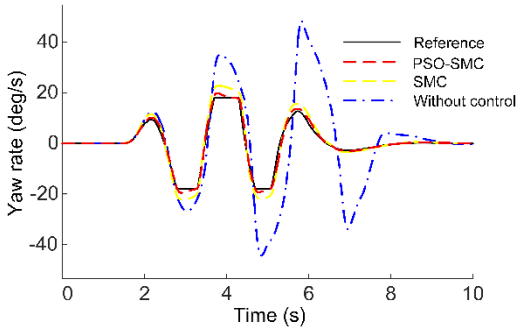
Fig. 5(a) shows the front steering angle input, providing typical steering dynamic excitation for the vehicle lateral dynamics under low-adhesion conditions. The yaw rate and CG sideslip angle responses in Fig. 5(b, c) indicate significantly improved tracking performance after applying control. As shown in Tab.4, compared with SMC, the proposed PSO-SMC effectively reduces E_{MAX}. Furthermore, the E_{RMS} of the yaw rate and CG sideslip angle are decreased by 32.3% and 37.1%, respectively. Fig. 5(d) illustrates the optimal torque allocated to the four wheels, which achieves differentiated coordinated regulation to accurately generate the desired additional yaw moment. These results demonstrate that the proposed strategy effectively enhances the lateral stability of the vehicle during high-speed driving under the low-adhesion DLC scenario.

4.1.2 Slalom Scenario

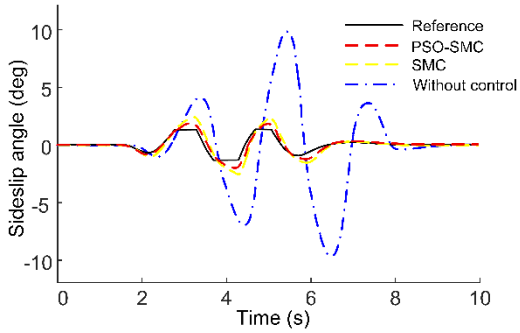
Simulations are conducted under the Slalom scenario with an initial speed of 85 km/h and road adhesion coefficients of 0.8 and 0.3. The results are shown in Fig. 6 and Fig. 7.



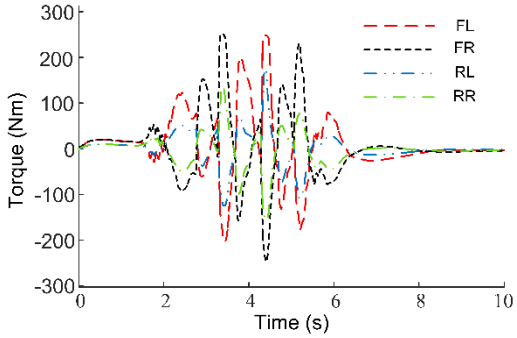
（a）Front wheel steering angle



（b）Yaw rate



（c）Sideslip angle



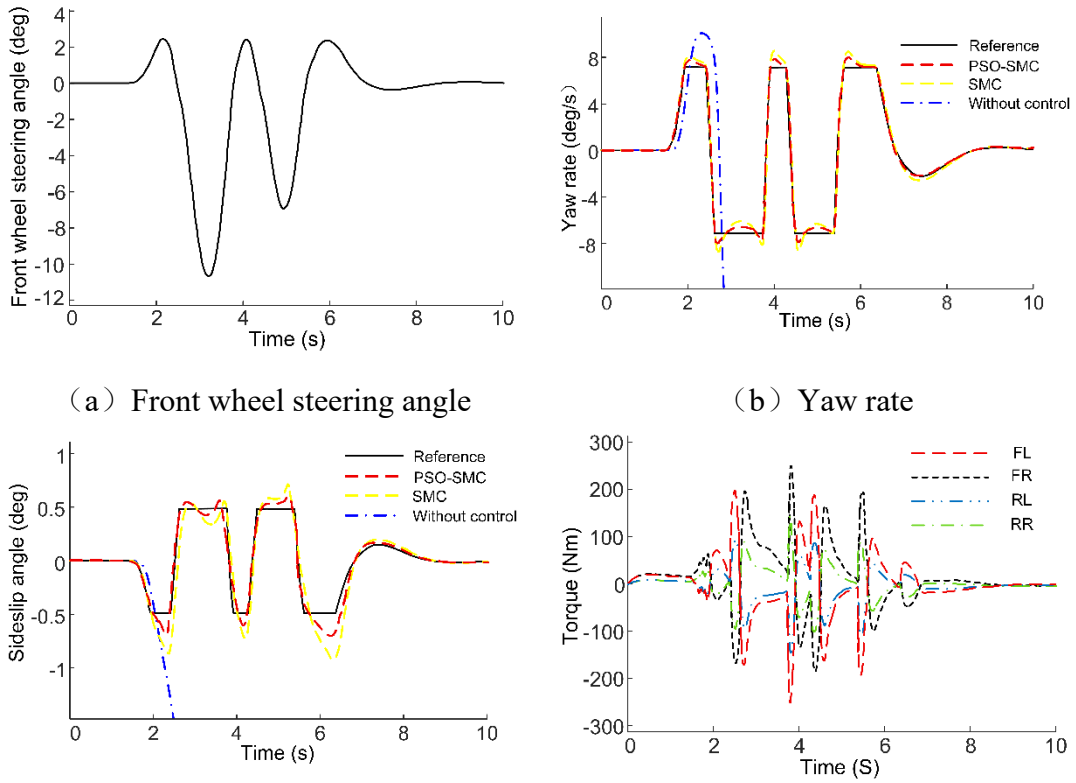
（d）Optimally distributed torque

Fig. 6 Simulation under Slalom scenario (μ = 0.8)

Tab.5 Slalom scenario errors (μ = 0.8)

Error	Control algorithm	Yaw rate (deg/s)	CG sideslip angle (deg)
E_{MAX}	SMC	4.557	1.026
	PSO-SMC	1.983	0.563
E_{RMS}	SMC	1.335	0.432
	PSO-SMC	0.714	0.221

Fig. 6(a) shows the front steering angle input, providing typical steering dynamic excitation for the vehicle lateral dynamics under low-adhesion conditions. The yaw rate and CG sideslip angle responses in Fig. 6(b, c) indicate significantly improved tracking performance after applying control. As shown in Table 5, compared with SMC, the proposed PSO-SMC effectively reduces E_{MAX}. Furthermore, the E_{RMS} of the yaw rate and CG sideslip angle are decreased by 46.5% and 48.8%, respectively. Fig. 6(d) illustrates the optimal allocated torque of the four wheels, achieving differentiated coordinated regulation of the four-wheel torques to accurately generate the desired additional yaw moment, ensuring the stable execution of the control strategy.



（a）Front wheel steering angle （b）Yaw rate

（c）Sideslip angle （d）Optimally distributed torque

Fig. 7 Simulation under Slalom scenario (μ = 0.3)

Fig. 7(a) shows the front steering angle input, where periodic continuous steering provides sustained dynamic excitation for the vehicle lateral dynamics under low-adhesion conditions. The yaw rate and CG sideslip angle responses in Fig. 7(b, c) demonstrate that both parameters lose control without intervention. After applying control, effective tracking is achieved, and the proposed PSO-SMC significantly outperforms the conventional SMC. Fig. 7(d) illustrates the four-wheel torque allocation, indicating that the lower-level controller dynamically regulates the torques according to low-adhesion limits to accurately generate the desired additional yaw moment. Therefore, under extreme low-adhesion continuous steering conditions, the designed control system effectively mitigates yaw instability and CG sideslip angle divergence, verifying its robustness and engineering applicability in complex extreme scenarios.

4.2 Hardware-in-the-loop Test

Compared with offline software simulations, hardware-in-the-loop (HIL) testing integrates physical hardware controllers and communication devices to enable real-time algorithm execution and data interaction. This approach avoids the risks of real-vehicle testing and supports repeated validation, thereby shortening the development cycle. In this section, an HIL test platform for DDEV lateral stability control is established based

on the NI PXI real-time simulator, as shown in Fig. 8.

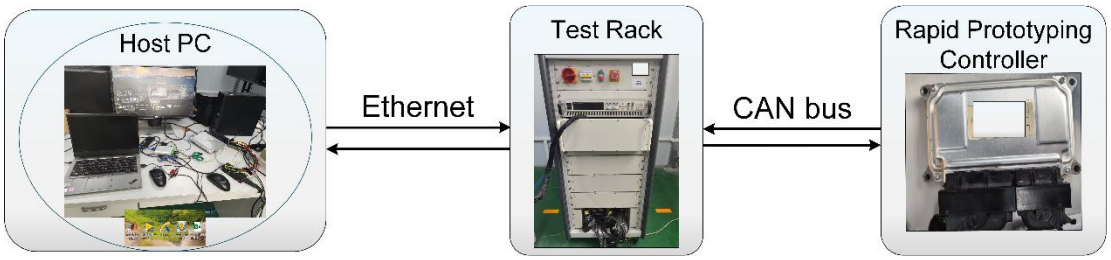
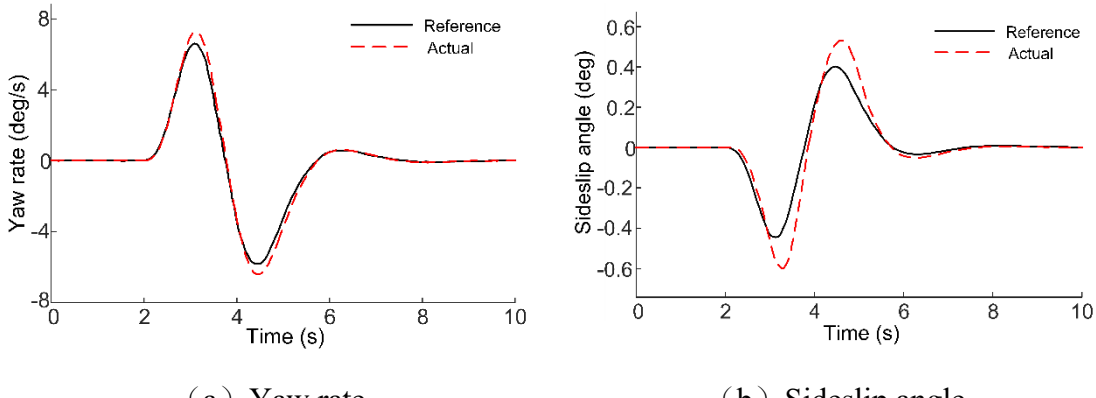


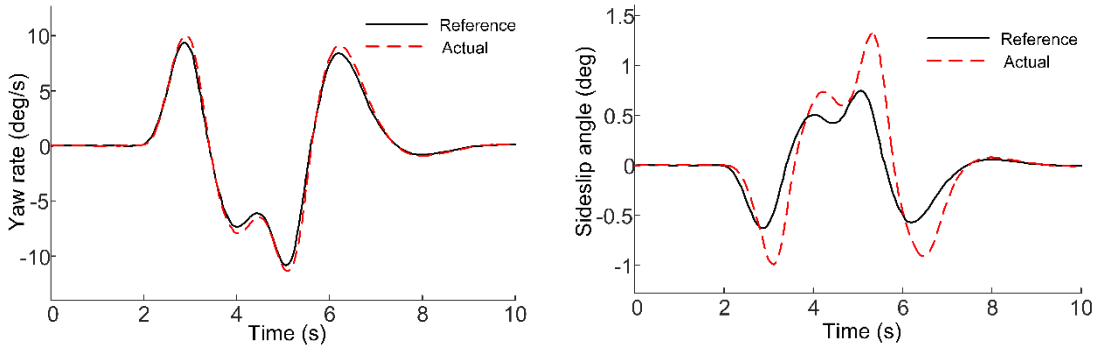
Fig. 8 HIL test platform

Based on the established HIL test platform, the proposed lateral stability control algorithm is experimentally validated under three typical scenarios: single lane change (SLC), DLC, and slalom. These correspond to real-world driving scenarios of single lane change, continuous lane change, and continuous steering, respectively. The initial speed is set to 85 km/h, and the road adhesion coefficient is set to 0.5. As shown in Fig. 9, the control accuracy, real-time performance, and robustness of the controller are verified by evaluating the tracking performance of the yaw rate and CG sideslip angle against their ideal reference values.



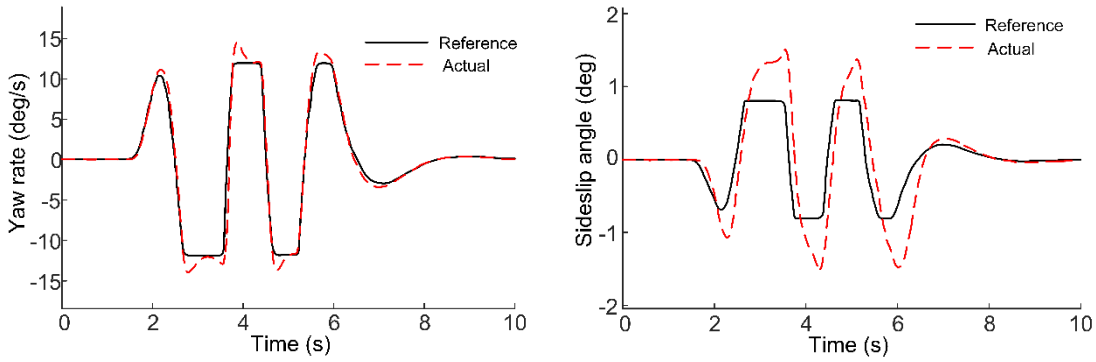
（a）Yaw rate

（b）Sideslip angle



（c）Yaw rate

（d）Sideslip angle



（e）Yaw rate　　（f）Sideslip angle

Fig. 9 Comparison of yaw rate and CG sideslip angle control performance under three scenarios

Under extreme driving conditions (85 km/h, road adhesion coefficient of 0.5), the proposed controller successfully tracks the yaw rate and CG sideslip angle references in the SLC, DLC, and slalom scenarios, verifying its effectiveness and robustness. However, the control accuracy exhibits a gradient variation across different maneuvers. In the SLC scenario, the actual curves nearly coincide with the references with no obvious lag, and the maximum peak deviations of the yaw rate and CG sideslip angle are only 0.604 deg/s and 0.131 deg, respectively, demonstrating high-precision tracking under simple steering. In the DLC scenario, slight deviations occur at the steering switching instants, but the overall trends remain highly consistent, with maximum deviations not exceeding 0.647 deg/s and 0.668 deg. In the slalom scenario, the actual curves fluctuate slightly around the references without divergence, as high-frequency reciprocal steering causes continuous dynamic variations and slight tracking lag; nevertheless, the maximum deviations of the yaw rate and CG sideslip angle remain within 2.466 deg/s and 0.787 deg, reflecting excellent stability under complex dynamic maneuvers.

5. Conclusion

Dynamic models are developed to improve the lateral stability of distributed-drive electric vehicles under complex operating conditions. By incorporating the road adhesion limit, ideal reference values for the yaw rate and the center-of-mass side slip angle are determined. A sliding-mode controller, whose control parameters are tuned via a particle swarm optimization algorithm, is designed with an additional yaw moment term. The phase-plane method is introduced to quantitatively determine the vehicle's steady-state operating conditions, and the final output target torque is adaptively adjusted using weighting coefficients.

Aiming to minimize the tire load rate, this controller integrates motor output limits and road adhesion constraints to develop an optimal quadratic programming-based

four-wheel torque distribution strategy, which enables precise allocation of the additional yaw moment.

Using the integrated CarSim–MATLAB/Simulink simulation platform, we conducted simulation tests of the proposed control algorithm under different road adhesion coefficients, covering both double lane change and snake driving conditions, and verified the rationality of the established model. The results demonstrate that, when comparing the improved PSO-SMC, conventional SMC, and the no-control scenario, the direct yaw moment controller and the moment distribution algorithm proposed in this study exhibit higher stability and outperform conventional SMC under all types of adhesion conditions.

Using the established HIL test platform, experimental validation is conducted on the lateral stability control algorithm under complex operating conditions. By comparing the tracking performance of actual control values versus ideal reference values for the yaw rate and the center-of-mass side slip angle under both single- and double-lane-change scenarios, the controller's control accuracy, real-time performance, and robustness are verified, confirming the approach delivers excellent vehicle speed tracking capability and stability.

The main limitation is that under the snake-shaped operating condition, the actual response curve fluctuates slightly around the reference curve; the deviation is marginally larger than that observed under the other two operating conditions, indicating a mild tracking lag that requires further improvement.

References

[1] XUAN Z, SHU W, JIAN M, et al. Review of Chassis Integrated Control Technology for Distributed Drive Electric Vehicles[Z]//China Journal of Highway and Transport. 2023.

[2] YIN Guo-dong,JIN Xian-jian， ZHANG Yun.Overview for Chassis Vehicle Dynamics Control of Distributed Drive Electric Vehicle[J].Journal of Chongqing University of Technology(Natural Science),2016,30(8):13-19+26.

[3] LI C, LIU H, HAN L, et al. Multi-Level Coordinated Yaw Stability Control Based on Sliding Mode Predictive Control for Distributed Drive Electric Vehicles Under Extreme Conditions[J]. IEEE Transactions on Vehicular Technology, 2023, 72(1): 280-296.

[4] LIU J, DAI A. Distributed-Drive Vehicle Lateral-Stability Coordinated Control Based on Phase-Plane Stability Region[J]. World Electric Vehicle Journal, 2024, 15(5): 202.

[5] Wei Z, Guizhen Y, Jian W, et al. Self-tuning fuzzy PID applied to direct yaw moment control for vehicle stability[C]//2009 9th International Conference on

Electronic Measurement & Instruments. IEEE, 2009: 2-257-2-261.
[6] ZHAO Huiyong,LIANG Guocai ,CAI Shuo , et al.Direct Yaw Moment Control for Four-Wheel Independent Drive Electric Vehicle[J].Journal of Chongqing University of Technology(Natural Science),2021,35(09):83-91.
[7] WU Jianyang, WANG Zhenpo, ZHANG Lei, et al.Coordination Stability Control Strategy for Four-wheel-independent-actuated Electric Vehicles[J].JOURNAL OF MECHANICAL ENGINEERING.2023,59(04):163-172.
[8] Siampis E, Velenis E, Gariuolo S, et al. A real-time nonlinear model predictive control strategy for stabilization of an electric vehicle at the limits of handling[J]. IEEE Transactions on Control Systems Technology, 2017, 26(6): 1982-1994.
[9] YAN Yun-bing,YI Zhen-yu,YANG Yong.Stability Control of Four-Wheel Independent Drive Electric Vehicle on Low Adhesion Road[J].Machinery Design & Manufacture,2022,(09):175-179+184.
[10] REN Zhengya,ZHAO Weiqiang,ZONG Changf,et al．Research on vehicle yaw stability control based on improved LQR method［J］．Science Technology and Engineering,2017,17(21) : 97-102.
[11] Tota A, Lenzo B, Lu Q, et al. On the experimental analysis of integral sliding modes for yaw rate and sideslip control of an electric vehicle with multiple motors[J]. International Journal of Automotive Technology, 2018, 19(5): 811-823.
[12] ZHANG Zheng,A Xiaojun,LIU Chunguang,et al.Direct Yaw Moment Control Based on Hierarchical Model for In-wheel Motor Drive Vehicles[J].Transactions of the Chinese Society for Agricultural Machinery,2019,50(12):387-394.
[13] Zhai L, Wang C, Hou Y, et al. MPC-based integrated control of trajectory tracking and handling stability for intelligent driving vehicle driven by four hub motor[J]. IEEE transactions on vehicular technology, 2022, 71(3): 2668-2680.
[14] Chen J, Lin C, Liang S. Mixed logical dynamical model-based MPC for yaw stability control of distributed drive electric vehicles[J]. Energy Procedia, 2019, 158: 2518-2523.
[15] YU Zhisheng．Automobile Theory［M］．Beijing：Mechanical Industry Press，2009：144-146.
[16] Zhang L, Chen H, Huang Y, et al. Human-centered torque vectoring control for distributed drive electric vehicle considering driving characteristics[J]. IEEE Transactions on Vehicular Technology, 2021, 70(8): 7386-7399.
[17] Zhao L H, Liu Z Y, Chen H. Design of a nonlinear observer for vehicle velocity estimation and experiments[J]. IEEE Transactions on Control Systems Technology, 2010, 19(3): 664-672.
[18] YANG Long.Direct Yaw Moment Control for In-wheel Motor Electric Vehicles[D].Chongqing University,2016.

Declarations：

Competing Interests：The authors declare that there are no competing financial interests or personal relationships that could have appeared to influence the work reported in this paper.

Data and Materials Availability：The datasets generated and/or analysed during the current study are not publicly available due to the confidentiality of the vehicle simulation model, bsut are available from the corresponding author on reasonable request.